

Off-Axis Properties of Silicon and Quartz Dielectric Lens Antennas

Daniel F. Filipovic, *Member, IEEE*, Gildas P. Gauthier, *Student Member, IEEE*,
Sanjay Raman, *Student Member, IEEE*, and Gabriel M. Rebeiz, *Fellow, IEEE*

Abstract—In this paper, the theoretical far-field patterns and Gaussian-beam coupling efficiencies are investigated for a double-slot antenna placed off axis on extended hemispherical silicon and quartz lenses. Measured off-axis radiation patterns at 250 GHz agree well with the theory. Results are presented that show important parameters versus off-axis displacement: scan angle, directivity, Gaussicity, and reflection loss. Directivity contour plots are also presented and show that near-diffraction limited performance can be achieved at off-axis positions at nonelliptical extension lengths. Some design rules are discussed for imaging arrays on dielectric lens antennas.

Index Terms—Dielectric antennas.

I. INTRODUCTION

A convenient method to eliminate substrate modes with integrated antennas is to place the antenna on a dielectric lens [1]. If the dielectric lens has the same dielectric constant as the planar antenna wafer, then substrate modes will not exist. In addition, antennas placed on dielectric lenses tend to radiate most of their power into the lens side, making the pattern unidirectional on high-dielectric constant lenses. The ratio of powers between the dielectric and air is approximately $\epsilon_r^{3/2}$ for elementary slot and dipole-type antennas [1] where ϵ_r is the relative dielectric constant of the lens. The dielectric lens also provides mechanical rigidity and thermal stability, and has been used extensively in millimeter- and submillimeter-wave receivers [2]–[8].

Previous investigations [2], [3], [9] have shown that the directivity of the substrate lens can be controlled by increasing or decreasing the extension length L , defined in Fig. 1. In particular, as the extension length increases from the hyperhemispherical length R/n (where R is the radius and n is the index of refraction of the lens), the directivity increases until it reaches a maximum diffraction-limited value. At the extension length, which realizes this maximum directivity, the extended hemispherical lens has a surface that closely approximates an elliptical lens with the planar antenna at the more distant focus.

While the directivity increases at higher extension lengths the pattern-to-pattern coupling value to a fundamental Gaussian-beam (Gaussicity) decreases [2]. Since the double-

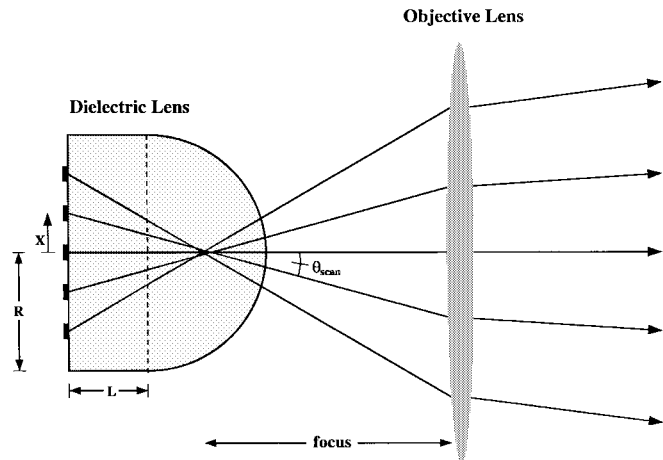


Fig. 1. A linear imaging array on an extended hemispherical dielectric lens coupled to an objective lens. The rays in this figure are not optically correct and are only meant for illustrative purposes.

slot antenna used in these studies launches a nearly perfect fundamental Gaussian-beam into the dielectric lens, the Gaussicity can also be thought of as a measure of the aberrations introduced by the lens. For extension lengths up to the hyperhemispherical position the Gaussicity is close to 100%. This is expected since the hyperhemispherical lens is aplanatic, implying the absence of spherical aberrations, and satisfies the sine condition, which guarantees the absence of circular coma [10]. As the extension length increases past R/n , the Gaussicity continuously decreases, which implies the introduction of more and more aberrations. Calculations in [2] and [9] indicate that for an “intermediate position” between the hyperhemispherical and diffraction-limited extension lengths ($L/R = 0.32$ to 0.35 for $\epsilon_r = 11.7$ and $L/R = 0.61$ to 0.76 for $\epsilon_r = 3.8$), the Gaussicity decreases by a small amount ($<10\%$), while the directivity is close to the diffraction-limited value. The choice of an “intermediate position” extension length has resulted in state of the art receivers at 90 and 250 GHz [5], [6].

This paper characterizes the off-axis performance of extended hemispherical dielectric lenses (Fig. 1). A ray-optics/field-integration formulation similar to that described in [2] is used to solve for the radiation patterns and Gaussian-coupling efficiencies. Briefly, the radiation of the feed antenna is ray traced to find the fields immediately exterior to the lens surface. For a given ray, the fields are decomposed into TE/TM components at the lens/air interface, and the

Manuscript received October 13, 1995; revised October 18, 1996. This work is supported by the NASA/Center for Space Terahertz Technology at the University of Michigan.

D. F. Filipovic is with Qualcomm Inc., San Diego, CA 92121 USA.

G. P. Gauthier, S. Raman, and G. M. Rebeiz are with the Department of Electrical Engineering and Computer Science, University of Michigan, Ann Arbor, MI 48109 USA.

Publisher Item Identifier S 0018-926X(97)03193-1.

appropriate transmission formulas are used for each mode. The equivalent electric and magnetic currents are found directly from the fields, and a standard diffraction integral results in the far-field lens patterns [11]. This general treatment results in the far-field lens patterns for any extension length, displacement, and orientation of the feed antenna with respect to the center of the lens. The characteristics for differing positions of the feed antenna are similar and this paper considers displacements for two cases: an E -plane scan, in which the feed is displaced in the direction of the E -plane and an H -plane scan in which the feed is displaced in the direction of the H plane.

In most applications the dielectric lens will be coupled with a quasi-optical system, and Fig. 1 shows the dielectric lens coupled to an objective lens. If the Gaussian beams emanating from the dielectric lens are well characterized, then one can easily trace these beams through a quasi-optical system [2], or for greater accuracy, the patterns emanating from the dielectric lens could be used with electromagnetic (EM) ray-tracing techniques to find the fields across the aperture of the objective lens. Then a Fourier transform will yield the far-field patterns from the objective lens/dielectric lens system.

II. THEORETICAL CALCULATIONS

The double-slot antenna patterns are calculated assuming a sinusoidal magnetic-current distribution on the slot and using an array factor in the E -plane direction [12]. The double slots lie in the x - z plane, and the slots point in the direction of the z axis. The wavelength of the sinusoidal magnetic-current distribution in the slot is approximately the geometric mean wavelength [13] given by $\lambda_m = \lambda_0/\sqrt{\epsilon_m}$ and $\epsilon_m = (1+\epsilon_r)/2$. The magnetic current in the slot is given by

$$I_m = I_{\max} \sin[k_m(l - |z|)], \quad -l \leq z \leq l, \quad 2l_{\max} = 0.28\lambda_{\text{air}} \quad (1)$$

where $k_m = 2\pi/\lambda_m$. The corresponding normalized H -plane field pattern is

$$\frac{\sin \theta [\cos(k_e l \cos \theta) - \cos(k_m l)]}{k_m^2 - k_e^2 \cos^2 \theta} \quad (2)$$

where $k_e = k_{\text{diel}} = 2\pi/\lambda_{\text{diel}}$ for the dielectric side, $k_e = 2\pi/\lambda_{\text{air}}$ for the air side, and θ is the angle with respect to the z axis. The element pattern is constant in the E plane. The E -plane array factor is given by

$$\cos\left(k_e \frac{d}{2} \sin \theta \cos \phi\right) \quad (3)$$

where ϕ is the angle from the x axis in the x - y plane, k_e is defined as above, and d is the spacing between the two slots.

All calculations are performed assuming a double-slot antenna as the feed antenna for the extended hemispherical dielectric lens. However, any antenna which illuminates the lens surface with a nearly symmetrical, equal-phase beam will produce similar results. The dimensions of the double-slot antenna are a length of $0.28\lambda_{\text{air}}$ and spacing of $0.16\lambda_{\text{air}}$ for a silicon lens ($\epsilon_r = 11.7$), and a length of $0.49\lambda_{\text{air}}$ and spacing of $0.28\lambda_{\text{air}}$ for a quartz lens ($\epsilon_r = 3.8$). The dimensions have been scaled according to the square root of the dielectric constant and yield nearly the same radiation patterns into the

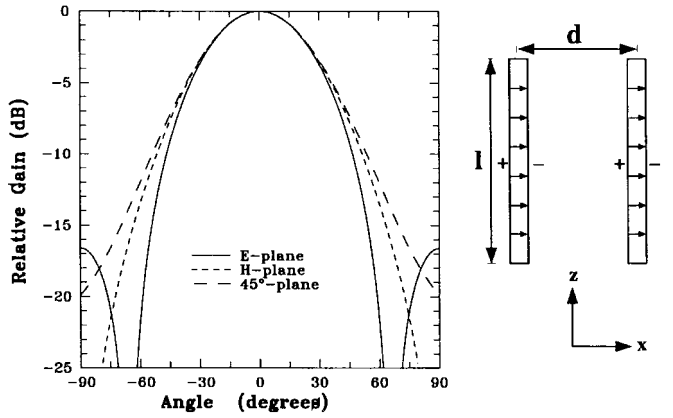


Fig. 2. The radiation patterns of the double-slot antenna into a silicon or quartz half-space.

respective lenses. The double-slot antennas (Fig. 2) produce symmetrical patterns into the infinite dielectric half-space with a corresponding directivity of 11.2 dB and a cross-polarization level lower than -23 dB in the 45° plane (the directivity quoted is calculated using the pattern radiated in the dielectric only). The radiation patterns are 98% Gaussian and, therefore, the radiation patterns from the dielectric lens should also have a Gaussicity of 98% if no aberrations are introduced. Note that the patterns radiated to the air-side are broader, and contain 9.0% of the total radiated power for a silicon lens and 28.3% of the total radiated power for a quartz lens. The theoretical technique for analyzing the lens-radiation patterns is an expanded version of the electromagnetic ray-tracing technique presented in [2]. The geometry of the problem is shown in Fig. 3 where the Cartesian axes have been reoriented so that the slots now lay in the x - y plane, and the z axis is, therefore, the central axis of the lens. First, define the surface normal to be

$$\hat{n} = \cos \theta \cos \phi \hat{x} + \cos \theta \sin \phi \hat{y} + \sin \theta \hat{z}. \quad (4)$$

Define the ray path inside the lens to be

$$\mathbf{v} = (x_s - dx)\hat{x} + (y_s - dy)\hat{y} + (z_s - dz)\hat{z} \quad (5)$$

$$\hat{v} = \mathbf{v}/|\mathbf{v}| \quad (6)$$

where (x_s, y_s, z_s) are the surface coordinates and (dx, dy, dz) are the feed location coordinates. The basis vectors that define the component of electric field that lies in either the perpendicular or parallel planes of incidence are

$$\mathbf{P}_\perp = \hat{n} \times \hat{v} \quad (7)$$

$$\hat{P}_\perp = \mathbf{P}_\perp / |\mathbf{P}_\perp| \quad (8)$$

$$\hat{P}_\parallel = \hat{P}_\perp \times \hat{v}. \quad (9)$$

Then the perpendicular and parallel values of electric field inside the sphere are

$$E_{\phi d} = \mathbf{E}_d \cdot \hat{P}_\perp \quad (10)$$

$$E_{\theta d} = \mathbf{E}_d \cdot \hat{P}_\parallel \quad (11)$$

where \mathbf{E}_d is the electric field on the lens surface *inside* the sphere, as calculated from (1)–(3). The electric field outside

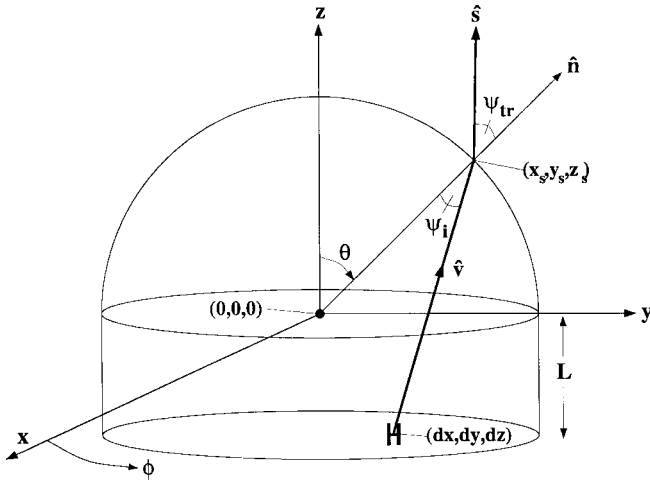


Fig. 3. The geometry used for the off-axis theoretical computations.

the sphere can then be derived to be

$$E_x = E_{\phi d} T_{\perp}(\hat{x} \cdot \hat{P}_{\perp}) + E_{\theta d} T_{\parallel} \times [(\hat{x} \cdot \hat{P}_{\parallel}) \cos(\psi_{tr} - \psi_i) - (\hat{x} \cdot \hat{v}) \sin(\psi_{tr} - \psi_i)] \quad (12)$$

$$E_y = E_{\phi d} T_{\perp}(\hat{y} \cdot \hat{P}_{\perp}) + E_{\theta d} T_{\parallel} \times [(\hat{y} \cdot \hat{P}_{\parallel}) \cos(\psi_{tr} - \psi_i) - (\hat{y} \cdot \hat{v}) \sin(\psi_{tr} - \psi_i)] \quad (13)$$

$$E_z = E_{\phi d} T_{\perp}(\hat{z} \cdot \hat{P}_{\perp}) + E_{\theta d} T_{\parallel} \times [(\hat{z} \cdot \hat{P}_{\parallel}) \cos(\psi_{tr} - \psi_i) - (\hat{z} \cdot \hat{v}) \sin(\psi_{tr} - \psi_i)] \quad (14)$$

$$\mathbf{E} = E_x \hat{x} + E_y \hat{y} + E_z \hat{z} \quad (15)$$

where ψ_i and ψ_{tr} are the angles of incidence and transmission, and T_{\perp} and T_{\parallel} are the perpendicular and parallel transmission coefficients at the lens-air interface defined in [2].

The ray path vector outside the lens can be found by

$$s_x = v_x \cos(\psi_{tr} - \psi_i) + (\hat{x} \cdot \hat{P}_{\parallel}) \sin(\psi_{tr} - \psi_i) \quad (16)$$

$$s_y = v_y \cos(\psi_{tr} - \psi_i) + (\hat{y} \cdot \hat{P}_{\parallel}) \sin(\psi_{tr} - \psi_i) \quad (17)$$

$$s_z = v_z \cos(\psi_{tr} - \psi_i) + (\hat{z} \cdot \hat{P}_{\parallel}) \sin(\psi_{tr} - \psi_i) \quad (18)$$

and, therefore, the magnetic field outside the sphere is simply

$$\mathbf{H} = \hat{s} \times \mathbf{E}. \quad (19)$$

Once the electric and magnetic fields are found just outside the sphere, the far-field is calculated using the Schellkunoff equivalence principle and standard far-field diffraction integrals [11] on the surface of the lens. The integrals are evaluated with respect to a coordinate system having its origin at the tip of the lens (see [2]). Thus, in subsequent calculations, the far-field phase or the near-field radius of curvature is always referenced to the tip of the lens.

Scan Angle: The resulting scan angle for an off-axis displacement X/R (where X is the distance off-axis and R is the radius of the lens) is shown in Fig. 4 at three different extension lengths L/R (where L is the extension length): hyperhemispherical, intermediate, and synthesized elliptical (diffraction-limited position), and for both silicon ($\epsilon_r = 11.7$) and quartz ($\epsilon_r = 3.8$) dielectric lenses. As expected, for a given X/R off-axis displacement, the silicon dielectric lens will have a larger scan angle than the quartz lens due to its

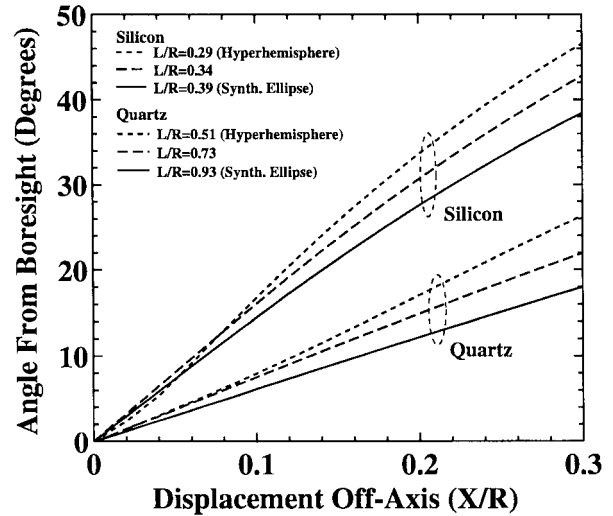


Fig. 4. Scan angle versus off-axis displacement at fixed extension lengths for a silicon and a quartz lens.

higher dielectric constant. Note that the off-axis positions are not dependent on the physical lens size. Also, the scan angle is independent of the direction of the displacement (i.e., E or H -plane scan).

Directivity: The effect of off-axis displacements on the directivity can best be seen by the contour plots for a $24\text{-}\lambda$ diameter silicon and quartz extended hemispherical dielectric lenses shown in Fig. 5. The contour plot for a quartz lens shows less variation in directivity off-axis than the silicon lens since the lower dielectric constant requires longer extension lengths, and thus lessens the effect of off-axis displacements. It is interesting to note that at the hyperhemispherical position ($L/R = 0.29$) for a $24\text{-}\lambda$ diameter silicon lens the patterns have higher directivity off-axis and achieve a maximum directivity of 35.2 dB at $X/R = 0.24$. This indicates that the diffraction-limited performance can be nearly achieved by either increasing the extension length on-axis past the hyperhemispherical position, or by moving the feed antenna position off-axis in the hyperhemispherical plane.

Gaussicity: Fig. 6 shows the Gaussicity plots for a $24\text{-}\lambda$ diameter silicon and quartz lens. Two types of Gaussicity are presented. The first set of curves represent the maximum Gaussicity available at a certain displacement (or a beam at a certain angle). The maximum Gaussicity is found by optimizing the Gaussian-beam parameters (waist and radius of curvature) at each displacement. In addition, the phase center (the point through which the axis of the Gaussian beam lies) is also changed to optimize the beam, however nearly the same result will be achieved if the phase center is assumed to be about $0.4R$ behind the tip of the lens (see Fig. 1). The maximum Gaussicity is useful for nonimaging applications in which there is a single beam at a specific location.

For imaging applications, in particular in a high $f/\#$ system (such as a radio telescope), the parameters of the incoming Gaussian beams are constant with off-axis displacement (at least over the typically narrow field of view). Therefore, the second set of curves is plotted to $0.1X/R$ using fixed Gaussian-beam parameters, and only for the synthesized el-

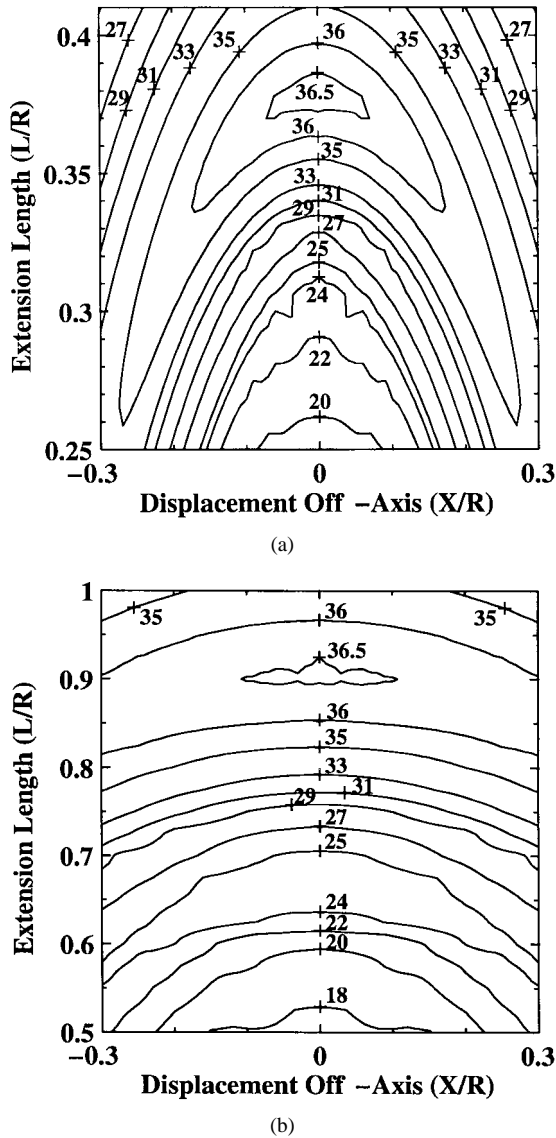


Fig. 5. Directivity contour plots of (a) silicon and (b) quartz versus extension length and off-axis displacement for a $24\text{-}\lambda$ diameter lens.

lindrical position since it provides the narrowest field of view from the substrate lens. The Gaussian-beam parameters that were used are presented in Table I, and they are the values that optimize the on-axis ($X/R = 0.0$) Gaussian beam. For the hyperhemispherical and intermediate positions, which do not have equiphase fronts, a full characterization of the system, including the objective lens, is needed.

Reflection Loss: The reflection loss for silicon and quartz lenses (independent of frequency or physical lens radius) is shown in Fig. 7 for off-axis displacements. As presented in [9], the reflection loss at the synthesized elliptical position is 0.5–1.0 dB higher than the hyperhemispherical position due to the power loss from the total internal reflection of wide angle rays. The reflection loss increases rapidly for a silicon lens after $X/R = 0.1$, while quartz lenses can be used up to $X/R = 0.25$ with less than a 1-dB increase in reflection loss. The reason for the rapid increase at off-axis positions in silicon is that an increased amount of the rays are being internally reflected. The loss curves are expected to be about

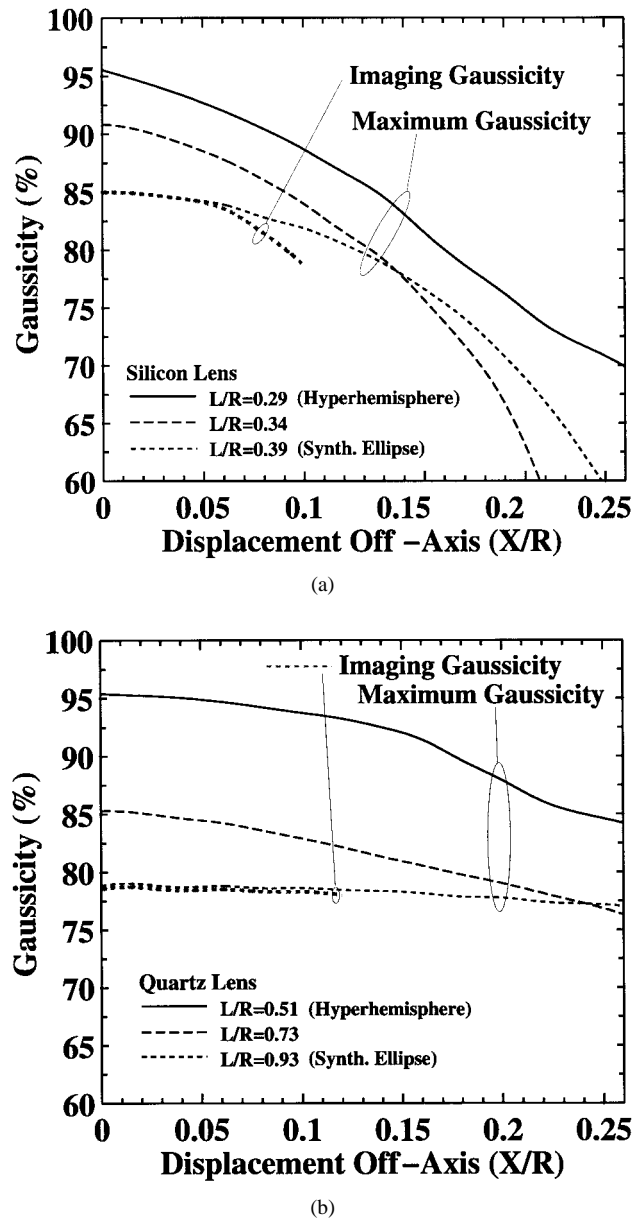


Fig. 6. Gaussicity versus off-axis displacement at fixed extension lengths for a $24\text{-}\lambda$ diameter (a) silicon and (b) quartz lens. The dark lines are maximum Gaussicity (variable Gaussian parameters) and the light lines are the Gaussicity using the on-axis Gaussian parameters.

TABLE I
ON-AXIS GAUSSIAN-BEAM PARAMETERS FOR A $24\text{-}\lambda$ DIAMETER LENS
(IN UNITS OF λ_{air}) AT THE SYNTHESIZED ELLIPTICAL POSITION

Silicon Lens		
Extension Length	$w(z)$	$R(z)$
L/R=.39	8.94	∞
Quartz Lens		
Extension Length	$w(z)$	$R(z)$
L/R=.93	9.43	∞

1.5–2.0 dB lower for a silicon lens and 0.6–0.7 dB lower for a quartz lens with a $\lambda_m/4$ matching cap layer, where $\lambda_m = \lambda_0/\sqrt{\epsilon_m}$ and $\epsilon_m = \sqrt{\epsilon_{\text{lens}}}$. The off-axis reflection loss without a matching-cap layer may be the limiting factor in the design of larger imaging arrays on dielectric lenses. The off-axis reflection loss is expected to be much lower for feed

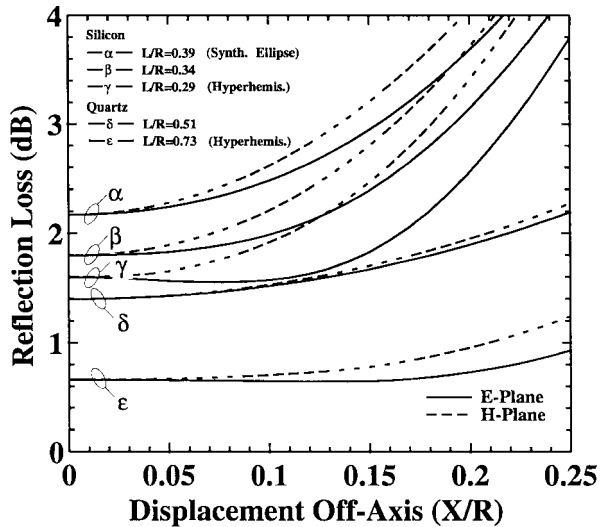


Fig. 7. Reflection loss versus off-axis displacement at fixed extension lengths for a silicon and quartz lens.

antennas having higher gain patterns (12–13 dB instead of 11 dB for double-slot antennas—see [2]).

III. MILLIMETER-WAVE MEASUREMENTS

In this section, a comprehensive set of radiation patterns at 250 GHz is presented for 13-element arrays at hyperhemispherical, intermediate, and synthesized elliptical positions. Two arrays were fabricated, one for an off-axis scan in the H plane, and one for an off-axis scan in the E plane. Only the H -plane scan results are presented since the E -plane scan results are very similar. Fig. 8 shows the vertical array for a scan in the H plane. The arrayed element is the double-slot antenna presented in Section II, with a length of $0.28 \lambda_{\text{air}}$ ($340 \mu\text{m}$) and a separation of $0.16 \lambda_{\text{air}}$ ($190 \mu\text{m}$). The double-slot antenna is integrated with a bismuth microbolometer at the center for detection [2]. Two capacitors are placed $\lambda_{\text{guide}}/2$ apart on the coplanar-waveguide line to short out the 250-GHz RF signal and pass only the low-frequency video signal. The element-to-element center spacing is chosen to be $0.35 \lambda_{\text{air}}$ ($420 \mu\text{m}$) for maximum packing efficiency. The array is placed on the back of a 13.7-mm diameter ($11.4 \lambda_{\text{air}}$ at 250 GHz) lens, and the middle element ($\#0$) of the 13-element array was aligned to the center of the lens. The array was measured at three extension lengths at 250 GHz to yield hyperhemispherical patterns ($L = 1.64 \text{ mm}$), intermediate patterns ($L = 2.18 \text{ mm}$), and diffraction-limited synthesized elliptical patterns ($L = 2.72 \text{ mm}$). No matching-cap layer was used on the silicon lens during the pattern measurements.

A comparison of the measured and theoretical radiation patterns at a low extension length of $L = 1.64 \text{ mm}$ ($L/R = 0.24$) is shown in Fig. 9. For this low X/R displacement, the radiation patterns are noisy because of a weak signal due to the low-directivity patterns and reflection on the lens-air interface. The fourth and fifth off-axis elements achieve a near diffraction-limited pattern (as predicted) and agree very well with the theory. Note also that the peak positions of the off-axis beams have been exactly predicted. Fig. 10

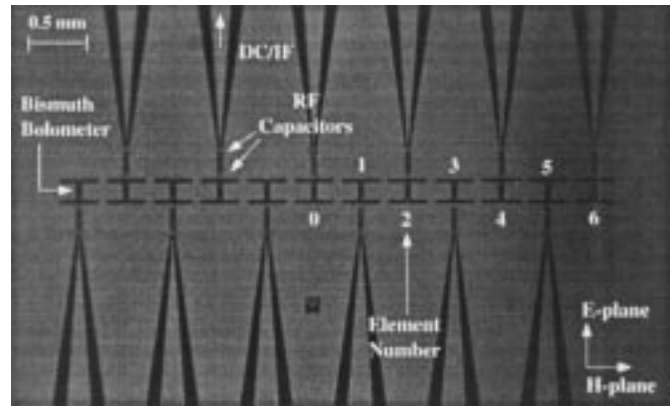


Fig. 8. The H -plane array for 250-GHz measurements. The element center-to-center spacing is $0.35 \lambda_{\text{air}}$.

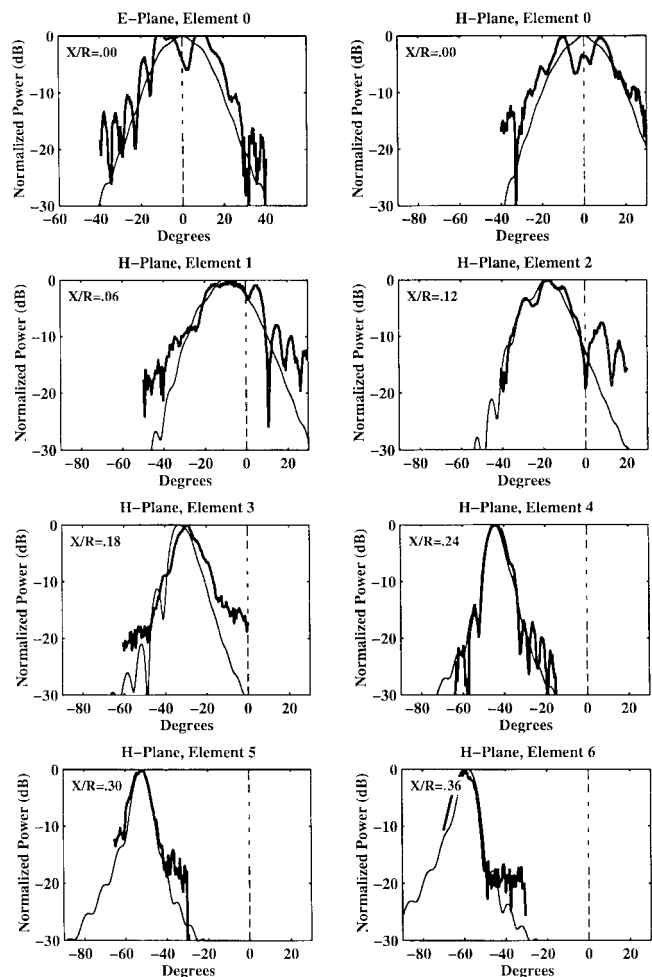


Fig. 9. Measured radiation patterns at 250 GHz for off-axis displacements at the hyperhemispherical position ($L/R = 0.24$) in the direction of the H plane. The lighter line is theory and the darker line is experiment.

compares the measured and theoretical radiation patterns at an intermediate extension length of $L = 2.18 \text{ mm}$ ($L/R = 0.32$). The diffraction-limited pattern occurs at the third-element off-axis, and note that the directivities are nearly constant for the first four off-axis elements. Fig. 11 compares the measured and theoretical radiation patterns at a synthesized elliptical extension length of $L = 2.72 \text{ mm}$ ($L/R = 0.40$). As expected,

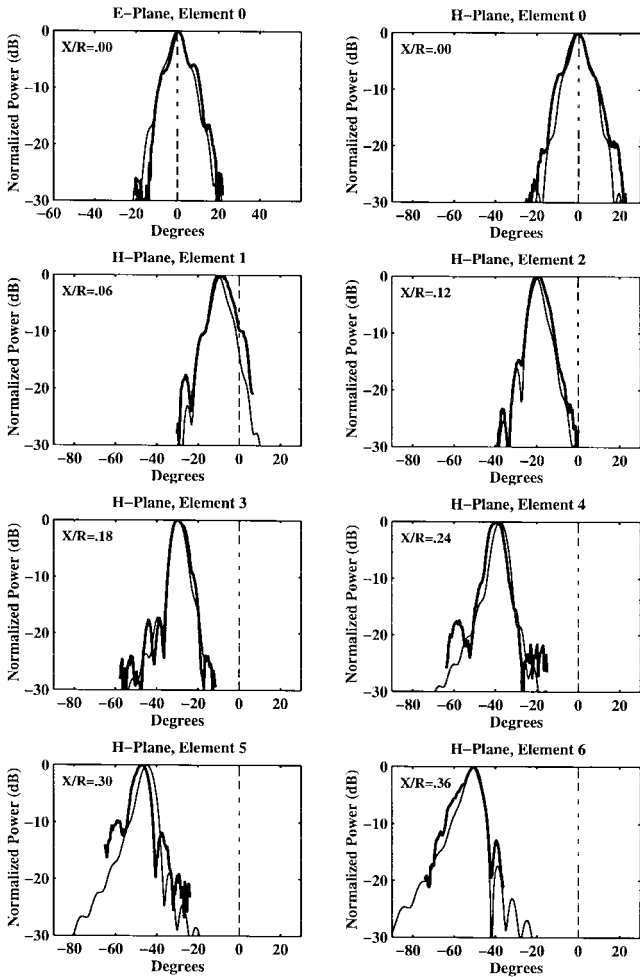


Fig. 10. Measured radiation patterns at 250 GHz for off-axis displacements at the intermediate position ($L/R = 0.32$) in the direction of the H plane. The lighter line is theory and the darker line is experiment.

the maximum directivity occurs on axis, and slowly decreases for off-axis positions, and there is good agreement between theory and experiment. The disagreements past 60° are due to lens blockage and/or mount reflections from the measurement fixture.

IV. CONCLUSION AND DISCUSSION

In this paper, design curves were presented for the important parameters versus off-axis displacement on a silicon and a quartz dielectric lens: scan angle, directivity, Gaussicity, and reflection loss. Contour plots were also presented that predict the exact directivity for any extension length and displacement for a silicon or quartz lens. These were experimentally verified at 250 GHz using an array in the E -plane direction and an array in the H -plane direction. It was shown that the directivity of a hyperhemispherical lens antenna increases for off-axis displacements. It was also found theoretically that for different types of lenses, an extension length just before the synthesized elliptical position maintains the directivity and the Gaussian-beam parameters the most constant. This was also shown experimentally with off-axis pattern measurements at intermediate and synthesized elliptical extension lengths.

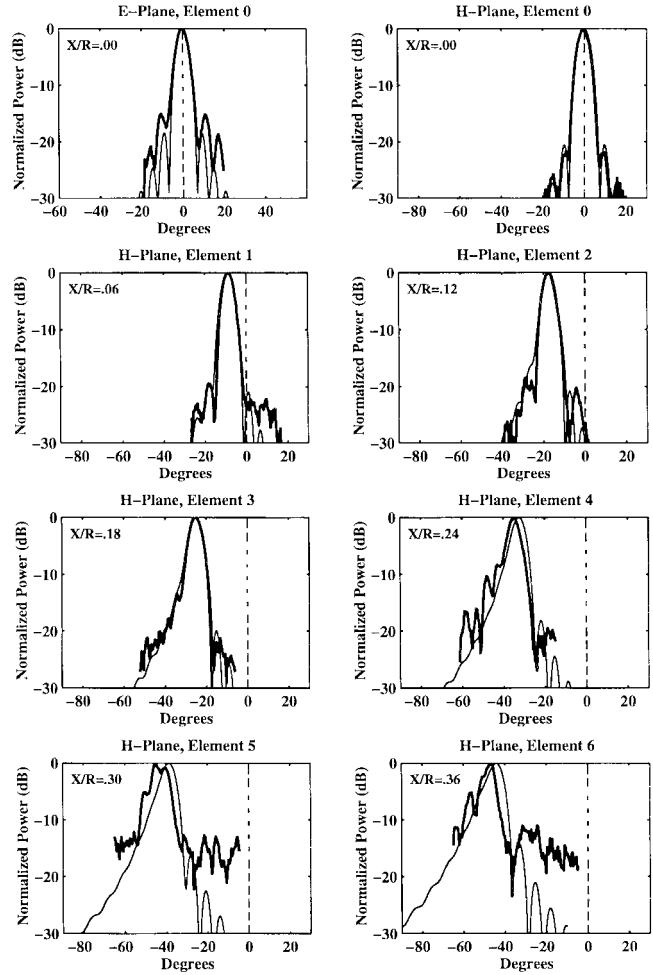


Fig. 11. Measured radiation patterns at 250 GHz for off-axis displacements at the elliptical position ($L/R = 0.40$) in the direction of the H plane. The lighter line is theory and the darker line is experiment.

Another discovery from the theoretical design curves is a constraint on the number of elements that can be packed into an imaging array. The maximum allowable value of X/R , without a *significant* increase in the reflection loss or decrease in the Gaussicity of the patterns is 0.12–0.14 for a silicon lens and 0.24–0.28 for a quartz lens. In both cases, this results in a maximum scan angle of around 20° , and the outer element will have a system coupling efficiency that is 0.7–1.2 dB lower than the center element (depending on the lens type and extension length value). For a silicon lens with a diameter of 24λ , this means that the maximum off-axis displacement is 1.45–1.7 λ_{air} on either side of the center element. Since double-slot or double-dipole antennas can be placed at a center-to-center spacing of 0.30–0.35 λ_{air} with low mutual coupling, the maximum number of elements for a 24λ diameter silicon lens is nine to eleven in a linear imaging array and 64–95 in a circular two-dimensional imaging array. Although the maximum allowable displacement is twice as large in a quartz lens, the planar antennas and the element-to-element spacing are also twice as large resulting in the *same* maximum allowed number of elements. The number of imaging elements can obviously be increased by increasing the physical size of the lens in wavelengths. However, it must be remembered that a

larger lens has a slightly lower on-axis Gaussicity [9] and will, therefore, shift lower the Gaussicity curves.

It is tempting to use very small antennas, such as a single dipole, a single slot, or a bow-tie antenna in an imaging array. The advantage is higher packing density and, therefore, more elements in the maximum allowable off-axis displacement region. However, there are two main disadvantages with this design. The first is that the Gaussicity of the element patterns in the lens is much lower (30–50% depending on the antenna), and the second is that these antennas suffer from more lens-air reflection losses in an extended hemispherical configuration due to their wide radiation patterns. In this case, it is recommended that small antennas be used exclusively at the hyperhemispherical extension length with the associated problems of aligning a large $f\#$ beam (from the telescope or primary lens) to an antenna array with very low directivity patterns.

REFERENCES

- [1] D. B. Rutledge, D. P. Neikirk, and D. P. Kasilingam, "Integrated circuit antennas," *Infrared and Millimeter-Waves*, K. J. Button, Ed. New York: Academic, 1983, vol. 10, pp. 1–90.
 - [2] D. F. Filipovic, S. S. Gearhart, and G. M. Rebeiz, "Double slot antennas on extended hemispherical and elliptical silicon dielectric lenses," *IEEE Trans. Microwave Theory Tech.*, vol. 41, pp. 1738–1749, Oct. 1991.
 - [3] T. H. Büttgenbach, "An improved solution for integrated array optics in quasioptical millimeter and submillimeter waves receivers: The hybrid antenna," *IEEE Trans. Microwave Theory Tech.*, vol. 41, pp. 1750–1761, Oct. 1991.
 - [4] J. Zmuidzinas, "Quasioptical slot antenna SIS mixers," *IEEE Trans. Microwave Theory Tech.*, vol. 40, pp. 1797–1804, Sept. 1991.
 - [5] G. P. Gauthier, W. Y. Ali-Ahmad, T. P. Budka, D. F. Filipovic, and G. M. Rebeiz, "A uniplanar 90 GHz Schottky-diode millimeter wave receiver," *IEEE Trans. Microwave Theory Tech.*, vol. 43, pp. 1669–1672, July 1995.
 - [6] S. S. Gearhart and G. M. Rebeiz, "A monolithic 250 GHz Schottky-diode receiver," *IEEE Trans. Microwave Theory Tech.*, vol. 42, pp. 2504–2511, Dec. 1994.
 - [7] H. Z. Zirath, C.-Y. Chi, N. Rorsman, and G. M. Rebeiz, "A 40-GHz integrated quasi-optical slot HFET mixer," *IEEE Trans. Microwave Theory Tech.*, vol. 42, pp. 2492–2497, Dec. 1994.
 - [8] A. Skalare, H. van de Stadt, Th. de Graauw, R. A. Panhuyzen, and M. M. T. M. Dierichs, "Double-dipole antenna SIS receivers at 100 and 400 GHz," in *Proc. 3rd Int. Conf. Space Terahertz Technol.*, Ann Arbor, MI, Mar. 1992, pp. 222–233.
 - [9] D. F. Filipovic and G. M. Rebeiz, "Double slot antennas on extended hemispherical and elliptical quartz dielectric lenses," *Int. J. Infrared Millimeter Waves*, vol. 14, pp. 1905–1924, Oct. 1991.
 - [10] M. Born and E. Wolf, *Principles of Optics*. New York: Pergamon, 1959, pp. 252–252.
 - [11] C. A. Balanis, *Antenna Theory: Analysis and Design*. New York: Wiley, 1982, ch. 11.
 - [12] R. S. Elliott, *Antenna Theory and Design*. Englewood Cliffs, NJ: Prentice-Hall, 1981, ch. 4.
 - [13] M. Kominami, D. M. Pozar, and D. H. Schaubert, "Dipole and slot elements and arrays on semi-infinite substrates," *IEEE Trans. Antennas Propagat.*, vol. AP-33, pp. 600–607, June 1985.
- Daniel F. Filipovic** (S'87–M'95) was born in Detroit, MI, on October 26, 1968. He received the B.S.E., M.S.E., and Ph.D. degree in electrical engineering from the University of Michigan, Ann Arbor, in 1990, 1991, and 1995, respectively. In 1994, he worked at Hughes Space and Communications, El Segundo, CA. In 1995 he joined Qualcomm, Inc., San Diego, CA, where he is currently developing antennas and RF circuitry for satellite communications.
- Gildas P. Gauthier** (S'96) was born in Angers, France, in 1969. He received the diploma of Telecommunications Engineer and the DEA from ENST Bretagne, Brest, France, in 1992. He is currently working toward the Ph.D. degree at the University of Michigan, Ann Arbor. From 1992 to 1994, he worked with IRAM, Grenada, Spain, on millimeter-wave superconductor-insulator-superconductor (SIS) receivers. His interests include microwave and millimeter-wave planar antennas and receivers.
- Sanjay Raman** (S'84) was born in Nottingham, U.K., on April 25, 1966. He received the B.E.E. degree (with highest honor) from the Georgia Institute of Technology, Atlanta, in 1987, and the M.S.E.E. degree from the University of Michigan, Ann Arbor, in 1993. He is currently working toward the Ph.D. degree in electrical engineering at the University of Michigan, Ann Arbor. From 1987 to 1992 he served as a nuclear-trained Submarine Officer in the U.S. Navy. In September 1992 he joined the EECS Department at the University of Michigan, Ann Arbor. His research interests include millimeter-wave receivers, antennas, radar systems, micromachining, and solid-state technology. Mr. Raman received the Best Student Paper Award at the 1995 IEEE Antennas and Propagation Symposium, Newport Beach, CA and at the 1996 IEEE International Microwave Symposium, San Francisco, CA.
- Gabriel M. Rebeiz** (S'86–M'88–SM'93) received the Ph.D. degree in electrical engineering from the California Institute of Technology, Pasadena, in 1988. He joined the faculty of the University of Michigan, Ann Arbor, in September 1988 and was promoted to Associate Professor in 1992. He is the author of 70 papers published in refereed journals and more than 110 papers presented in national and international conferences. His interests are in applying micromachining techniques in silicon and GaAs for the development of low-loss and low-cost microwave antennas, components, and subsystems for wireless applications and satellite communication systems. He is also interested in the development of planar collision-avoidance sensors for automotive applications and in millimeter-wave imaging arrays, monopulse tracking systems, and phased arrays. Dr. Rebeiz received the National Science Foundation Presidential Young Investigator Award in 1991 and the URSI International Isaac Koga Gold Medal Award for Outstanding International Research in 1993. He also received the Research Excellence Award in 1995 from the University of Michigan, Ann Arbor. Together with his students, he is the winner of Best Paper Awards at JINA 1990, IEEE-MTT 1992, 1994, 1995, 1996, and IEEE- AP 1992 and 1995. He is an elected member of URSI-D and was a Visiting Professor at Chalmers University of Technology (1992) and at the École Normale Supérieure (1993).